Bone 114 (2018) 206–214

Contents lists available at ScienceDirect

Bone

journal homepage: www.elsevier.com/locate/bone

Full Length Article

Quantification of bone microstructure in the wrist using cone-beam computed tomography

Karen Mys[a,*], Filip Stockmans[b], Evie Vereecke[b], G. Harry van Lenthe[a]

[a] Biomechanics Section, Department of Mechanical engineering, KU Leuven, Leuven, Belgium
[b] Muscles & Movement, Department of development and Regeneration, KU Leuven Campus Kulak, Kortrijk, Belgium

ARTICLE INFO

Keywords:
Cone-beam computed tomography
Bone parameters
Micro-computed tomography
Medical imaging processing
Quantification

ABSTRACT

Due to the rising life expectancy, bone diseases (e.g. osteoporosis, osteoarthritis) and trauma (e.g. fracture) have become an important socio-economic burden. Accurate visualization and quantification of the bone microstructure in vivo is seen as an important step to enhance diagnosis and treatment. Micro-computed tomography (microCT) has become the gold standard in three-dimensional (3D) imaging of trabecular bone structure. Yet, usage is limited to ex vivo analyses, hence, it cannot be used to evaluate bone and bone adaptive responses in a patient. High-resolution peripheral computed tomography (HR-pQCT) is considered the best technique to measure the bone microarchitecture in vivo. By design HR-pQCT is limited to scanning extremities, such as the distal radius and distal tibia with a limited field of view and long scanning time (~2 à 3 min. for a stack of 0.9 cm). Cone-beam computed tomography (CBCT) is a promising alternative with a much larger field of view. Yet, CBCT is challenged by artefacts that reduce image contrast, such that it is currently being used for qualitative evaluation only. Therefore, the aims of this work were first to enhance image contrast and second to determine the accuracy of high-resolution CBCT for bone microarchitectural assessment.

Trapezia of nineteen female arthritic patients were scanned twice ex vivo; once using CBCT (NewTom 5G, Cefla, Verona, Italy) at a nominal voxel size of 75 μm and once using microCT (SkyScan 1172, Bruker, Kontich, Belgium) at a voxel size of 19.84 μm. The CBCT-scans were reconstructed following 2 protocols: (1) using the commercial software delivered with the scanner and (2) using in-house developed software. After reconstruction and image processing, the images were segmented using adaptive thresholding. Bone morphometric parameters including bone volume (BV), total tissue volume (TV), bone volume fraction (BV/TV), bone surface density (BS/TV), trabecular thickness (Tb.Th), trabecular separation (Tb.Sp) and trabecular number (Tb.N) were calculated. Statistical evaluations were made at a significance level of 5%.

Significant correlations were found between the CBCT-based bone parameters and the microCT-based parameters with $R^2 > 0.68$ The in-house reconstructed software outperformed the commercial software. Smaller bias (overestimation of Tb.Th decreased from 114.24% to 59.96%) as well as higher correlations were observed for the in-house processed images. Still, a significant overestimation was observed for BV/TV and Tb.Th and an underestimation for Tb.N.

We conclude that our CBCT image reconstruction improved image contrast which allowed for an accurate quantification of trabecular bone microarchitecture.

1. Introduction

Due to the aging population, bone diseases such as osteoporosis and osteoarthritis, are causing an increased socio-economic burden [1]. Visualization and quantification of the bone microstructure is often seen as an important step for a better understanding, diagnosis and follow up of bone diseases [2]. Conventional medical imaging techniques, such as CT, X-ray and MRI, have important shortcomings when applied to the visualization of bone micro-architecture. Conventional CT and MRI can scan a large field of view, but its resolution (about 400 μm) is inadequate to depict individual trabeculae (thickness ~50 − 200 μm). X-ray imaging has a better resolution, but its application towards visualization and quantification of bone micro-architecture is limited due to the two-dimensional nature of the technique (projection images).

Several imaging techniques are currently being used to assess bone microarchitecture, of which micro-computed tomography (microCT) has become the gold standard [3]. MicroCT provides high-resolution, three-dimensional imaging of trabecular bone structure allowing

* Corresponding author.
E-mail address: kmys@myrosoft.com (K. Mys).

https://doi.org/10.1016/j.bone.2018.06.006
Received 8 March 2018; Received in revised form 15 May 2018; Accepted 10 June 2018
Available online 15 June 2018
8756-3282/

comparison between normal and diseased bone tissue. Yet, usage is limited to ex vivo analysis, hence, it cannot be used to evaluate bone microstructure and adaptive responses in vivo. In vivo analysis of bone structure at the distal forearm and ankle has recently become possible with the advent of high-resolution peripheral quantitative CT (HR-pQCT) [4–7]. Two systems are currently on the market (XtremeCT I + II, Scanco Medical, Brüttisellen, Switzerland), which provide a resolution up to 60.7 μm. So far, this imaging technique has mainly been used in a research context and has not found its way into daily clinical practice. One of the reasons for this is because scanning one stack of 0.9 cm takes 2 to 3 min., making in vivo scanning of larger volumes of interest challenging.

A relatively new alternative is high-resolution Cone-beam computed tomography (CBCT) [8]. It has become the gold standard in many dental and maxillofacial imaging applications due to its high spatial resolution and low radiation dose (around 14 μSv for a FOV of 12 × 8 [9]) [10–12]. CBCT for musculoskeletal applications became possible with the advent of systems that looked like a small CT and that could examine the patient in the supine position or systems with a ring design through which an arm or leg could be put. The imaging of the fingers, wrist, elbow, foot, ankle and knee joint using CBCT have been reported as well as imaging of long bones of the extremities [13]. Despite the promising characteristics of high-resolution CBCT-scanners, i.e. high spatial resolution (75 μm), low radiation dose, fast acquisition, high versatility and cost-effectiveness, the applicability of CBCT for musculoskeletal applications is still limited to qualitative analyses, mainly due to imaging artefacts that reduce image contrast. Furthermore, state-of-the-art CBCT-scanners are not calibrated to BMD. Therefore, the aims of this work were (1) to enhance image contrast and (2) to determine the accuracy of high-resolution CBCT for bone microarchitectural assessment.

2. Materials and methods

2.1. Sample collection

A total of 19 trapezia (12 right, 7 left; 18 female, 1 male) were removed from the hands of arthritic patients ranging in age from 53 to 76 years (mean 63.4 years) via trapeziectomy by a certified hand surgeon (FS). The samples were stored directly after the operation at −20°C and were thawed prior to further analyses.

2.2. Image acquisition

Each sample was scanned ex vivo using Cone-beam computed tomography (CBCT, NewTom 5G, Cefla, Italy) at 75 μm, which is the best possible voxel size of this device. Next, the samples were scanned using micro-computed tomography (microCT, SkyScan 1172, Bruker, Belgium) at a voxel size of 19.84 μm. The samples were put in phosphate buffered saline during microCT scanning to avoid dehydration (Table 1).

Table 1
Scanning parameters of the CBCT NewTom 5G (Cefla, Verona, Italy) and microCT Skyscan-1172 (Bruker, Kontich, Belgium).

	CBCT NewTom 5G	MicroCT Skyscan
Energy (kVp)	110	100
Current (μA)	7–13	100
FOV (cm × cm × cm)	6 × 6 × 6	2x2x1
Projections	486	512
Isotropic voxel size (μm)	75	19.84

2.3. Image processing

2.3.1. Image reconstruction

The processing and reconstruction of the projection data of the CBCT-images were performed using the reconstruction software provided with the scanner as well as using in-house developed reconstruction and image processing software (Fig. 1).

The in-house developed reconstruction started from the projection data. Firstly, filtering was performed to reduce the detector noise present in the projection data. Afterwards the polyenergetic ray sum, $p = -ln\left(\frac{I_D}{I_0}\right)$, was calculated from the transmitted flux, I_D, and the blank scan, I_0. The blank scan, $I_{0.}$, was obtained by making a second scan without the bone, but with the same scanner properties and the same bed position. The projection data was corrected for the current modulation which was present during scanning. Afterwards, the images were reconstructed at a slightly higher voxel size of 60 μm by making use of an in-house developed multithreaded FDK (Feldkamp, Davis and Kress) reconstruction program. A Ram-Lak high-pass filter [14] was applied in the reconstruction program. In a second step, beam hardening correction was performed using in-house developed software. No smoothing or other filtering was done during the reconstruction or processing of the data. For the remainder of this paper, the terms RManufacturer, RInHouse, and RInHouseBeam and will be used to identify the images reconstructed using the software that comes with the CBCT scanner, using our in-house algorithm, and using our in-house algorithm with beam hardening correction, respectively.

2.3.2. Image segmentation

Segmentation of the CBCT-images was implemented in the program CTan (Bruker, Kontich, Belgium) and is described in more detail in Appendix 1. The microCT-images were segmented with a fixed global threshold and the noise was removed using a despeckler.

2.4. Image analysis

For the microCT-images, the trabecular bone parameters were calculated in a trabecular volume of interest (VOI) that was determined automatically following the method described by Buie et al. [15]. The methodology, explained in more detail in Appendix 2, was adapted such that the technique could also be used for bones without a well-defined cortex.

Using CTan the following morphological parameters were calculated for the bone within the trabecular mask in a direct way using a 3D analysis: bone volume fraction (BV/TV), trabecular thickness (Tb.Th), trabecular separation (Tb.Sp) and trabecular number (Tb.N), bone surface density (BS/TV). These analyses were performed for all image data, i.e., microCT, RManufacturer, RInHouse, and RInHousebeam.

2.5. Statistical analysis

Statistical analyses were performed in Matlab (The Mathworks, Natick, United States). To compare microarchitectural parameters obtained with each imaging protocol, linear regression was performed and the relative error (δe) was calculated. For the statistical tests, the confidence level α was set to 5%. Finally, trendlines and Bland–Altman plots were generated for RInHouseBeam to assess the accuracy of CBCT in measuring the microstructural parameters. [17, 18].

3. Results

Table 2 shows the coefficients of determination between the microstructural parameters as obtained from MicroCT and those obtained from RManufacturer, RInHouse and RInHouseBeam, respectively. Regression and Bland Altman plots between MicroCT and RInHouseBeam are shown in Fig. 2.

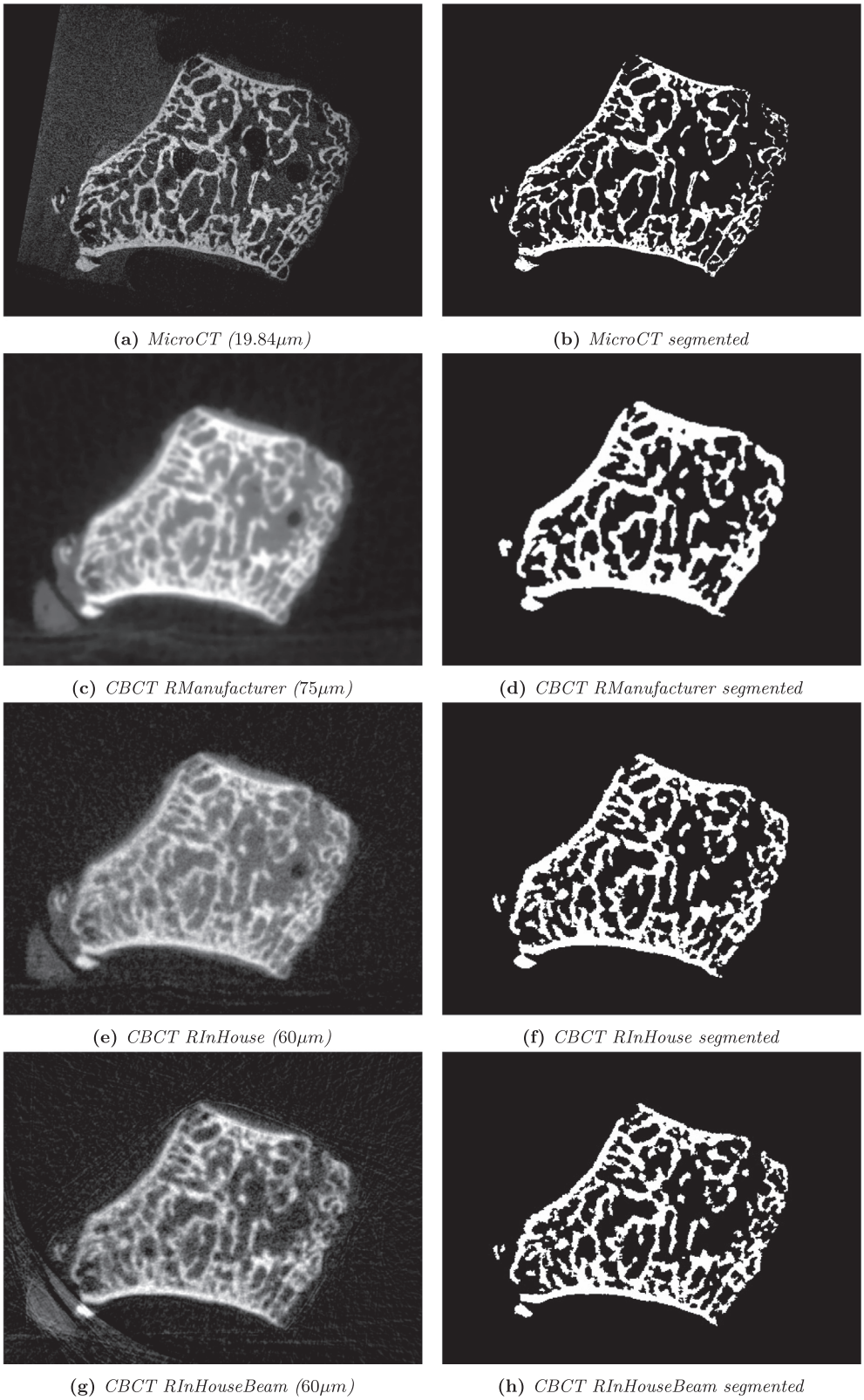

(a) *MicroCT (19.84μm)* (b) *MicroCT segmented*

(c) *CBCT RManufacturer (75μm)* (d) *CBCT RManufacturer segmented*

(e) *CBCT RInHouse (60μm)* (f) *CBCT RInHouse segmented*

(g) *CBCT RInHouseBeam (60μm)* (h) *CBCT RInHouseBeam segmented*

Fig. 1. The reconstructed images (a, c, e, g) and the corresponding segmented images (b, d, f, h). (a, b) microCT-image; (c,d) CBCT-image reconstructed using the standard scanner software (RManufacturer); (e, f) in-house reconstructed image (RInHouse); (g, h) in-house reconstructed image with beam-hardening correction.

Bone volume fraction (BV/TV), as determined using RInHouse and RInHouseBeam, was highly correlated with the microCT analyses (Fig. 2a) though CBCT overestimated BV/TV. A much higher correlation and smaller bias was observed for RInHouseBeam (R^2 = 0.69; $\delta\epsilon$ = 38.33%) than for the two other protocols, RInHouse (R^2 = 0.65; $\delta\epsilon$ = 48.20%) and RManufacturer (R^2 = 0.60; $\delta\epsilon$ = 55.14%).

All CBCT protocols significantly overestimated trabecular thickness (Fig. 2b). The in-house reconstruction protocols (RInHouse and

Table 2
Relative error (δe) with standard deviation and coefficients of determination between microCT and RManufacturer (standard scanner's reconstruction), RInHouse (in house reconstruction) and RInHouseBeam (in house reconstruction with beam hardening correction) for all samples ($N = 19$). RInHouseBeam outperformed RManufacturer and provided smaller bias as well as higher correlations.

	CBCT (N = 19)						
	MicroCT	RManufacturer		RInHouse		RInHouseBeam	
	Mean(SD)	$\delta\epsilon$(SD)	R^2	$\delta\epsilon$(SD)	R^2	$\delta\epsilon$(SD)	R^2
BV/TV [%]	23.38(2.8)	55.14(11.5)%	0.60	48.20(10.4)%	0.65	38.33(9.9)%	0.69
Tb.Th [mm]	0.18(0.02)	114.24(17.9)%	0.52	66.39(11.0)%	0.68	59.96(10.2)%	0.68
Tb.Sp [mm]	0.61(0.07)	9.43(5.7)%	0.84	−4.45(5.4)%	0.81	0.98(7.0)%	0.73
Tb.N [1/mm]	1.30(0.11)	−27.74(3.4)%	0.63	−10.91(3.3)%	0.82	−13.53(4.0)%	0.81
BS/TV [1/mm]	4.79(0.35)	−28.99(3.5)%	0.50	−9.7(4.0)%	0.72	−10.45(4.5)%	0.72

RInHouseBeam) overestimated the trabecular thickness (Tb.Th) with an average of 108μm ($\delta e = 59.96\%$) and 120 μm ($\delta e = 66.39\%$), respectively, whereas the average overestimation was 206 μm ($\delta e = 114.24\%$) when the scanner's reconstruction (RManufacturer) was used.

Trabecular separation (Tb.Sp) was highly correlated with the results obtained via microCT, and this for all the reconstructions (Fig. 2c). Tb.Sp was slightly underestimated ($\delta e = -4.45\%$) by RInHouse and slightly overestimated by RInHouseBeam ($\delta e = 0.98\%$), respectively. The reconstructed images by the scanners software (RManufacturer) overestimated Tb.Sp ($\delta e = 9.43\%$).

Trabecular number (Tb.N) (Fig. 2d) calculated from CBCT images was highly correlated with the data obtained from microCT, for all reconstructions. A higher bias was observed for RManufacturer ($\delta e = -27.74\%$) than for the in-house reconstruction ($\delta e = -10.91\%$ for RInHouse and $\delta e = -13.53\%$ for RInhouseBeam).

A high correlation was observed between bone surface (BS/TV) (Fig. 2e) obtained from the CBCT- and microCT-images. RInHouse ($\delta e = -9.7\%$) and RInHouseBeam ($\delta e = -10.45\%$) and slightly underestimated the BS/TV. The bias was substantially higher ($\delta e = -28.99\%$) when the reconstruction by the manufacturer was used.

4. Discussion

The aims of this study were (1) to enhance image contrast and (2) to determine the accuracy of high-resolution CBCT for bone microarchitectural assessment. Both aims have been achieved. For the first aim, we implemented a multithreaded C++ code to process the projection data, to reconstruct a 3D-image and to perform image correction afterwards. For the second aim, we determined the accuracy using a sample of 19 fresh-frozen arthritic trapezia which were scanned ex vivo using both CBCT and microCT. This means that a relevant group of subjects (osteoarthritic patients) as well as well-conserved bones (fresh frozen bone) were used in this study.

We demonstrated that the in-house processed images (RInHouse and RInHouseBeam) outperformed the reconstructed images using the scanner's reconstruction software (RManufacturer). Higher correlations and smaller bias (systematic smaller over- or underestimation) were obtained. The beam hardening correction applied in RInHouseBeam decreased the bias significantly against RInHouse. Tb.Sp was slightly underestimated ($\delta e = -4.45\%$) by RInHouse and slightly overestimated by RInHouseBeam ($\delta e = 0.98\%$), respectively. This is in accordance with an overestimation of Tb.Th. In contrast to the in-house processed images, RManufacturer overestimated Tb.Sp significantly ($\delta e = 9.43\%$). This can be explained by the large number of thin trabeculae that were not detected in RManufacturer as well as by the presence of spatially closely related trabeculae that were depicted as one thick trabeculae instead.

We also demonstrated that CBCT has a high potential to visualize and quantify the bone microstructure for musculoskeletal applications. Significant correlations between the CBCT-images and the microCT-images were observed for all bone parameters (BV/TV, BS/TV, Tb.Th, Tb.Sp and Tb.N).

An additional strength of this study was that the segmentation of all the images was done following automated protocols in a completely automatic way that did not require any user interaction. Not only did this eliminate the subjective impact of interpretation, it also eliminated the tedious and time-consuming masking procedure.

This is the first study to report on the quantification of bone microstructure using CBCT for musculoskeletal applications. A few studies have presented CBCT-based bone microstructure for dental applications [12, 19, 20]. In the analyses for dental purposes, the overestimation in Tb.Th was at least 184% [19] and 112% [20]. The latter corresponds quite well to the overestimation found for RManufacturer (114.24%) in our study. In the present study, we found an overestimation of 59.96% when using the RInHouseBeam protocol which represents an important improvement compared to the previous studies. Furthermore, the correlations obtained in the present study are among the highest published in literature [19, 20]. In addition, it should be noted that in the present study fresh-frozen trapezia of severely osteoarthritic patients were used whereas dry defatted bones were used in the dental applications. We hypothesize that the segmentation of defatted bone is easier than the bones used here because the image contrast between bone and soft tissue is smaller than the contrast between bone and air. The use of severely osteoarthritic bones with large variations in trabecular thickness is likely to have complicated the segmentation; hence, we hypothesize that the analyses of the trapezia represents a more challenging case than those of the bones for dental applications. Yet, considering the use of samples from other anatomical locations and considering that in the present study we used severely osteoarthritic bone, limits a direct comparison to previous studies.

An alternative to using CBCT in the visualization and quantification of bone microstructure is using high-resolution peripheral quantitative computed tomography (HR-pQCT). The correlations achieved in this study were higher than those obtained using the first generation HR-pQCT (XTremeCT, voxel size 82 μm) [21] (analysed using direct voxel-based measurements of structure), but inferior to the second generation HR-pQCT (XTremeCT-II, voxel size 61 μm) [22]. Yet, because the HR-pQCT studies have evaluated other anatomical sites than we evaluated using CBCT, a direct comparison cannot be made. In future work, we will extend our comparison to HR-pQCT.

Three trapezia contained a microstructure that was characterized by many thin trabeculae, defined as containing > 40% of the trabeculae with a thickness below 120μm, which represents < 2 voxels in the in-house reconstructed CBCT-images. Those bones were marked in Fig. 2 and all analyses were repeated with those three samples excluded (Table 3). Those images appeared blurry and could not be segmented accurately. Indeed, the coefficients of determinations were in general higher when those bones were excluded. An exception was Tb.Th; due to the exclusion of the three samples with the lowest trabecular thickness, the spread in values became smaller leading to a lower coefficient

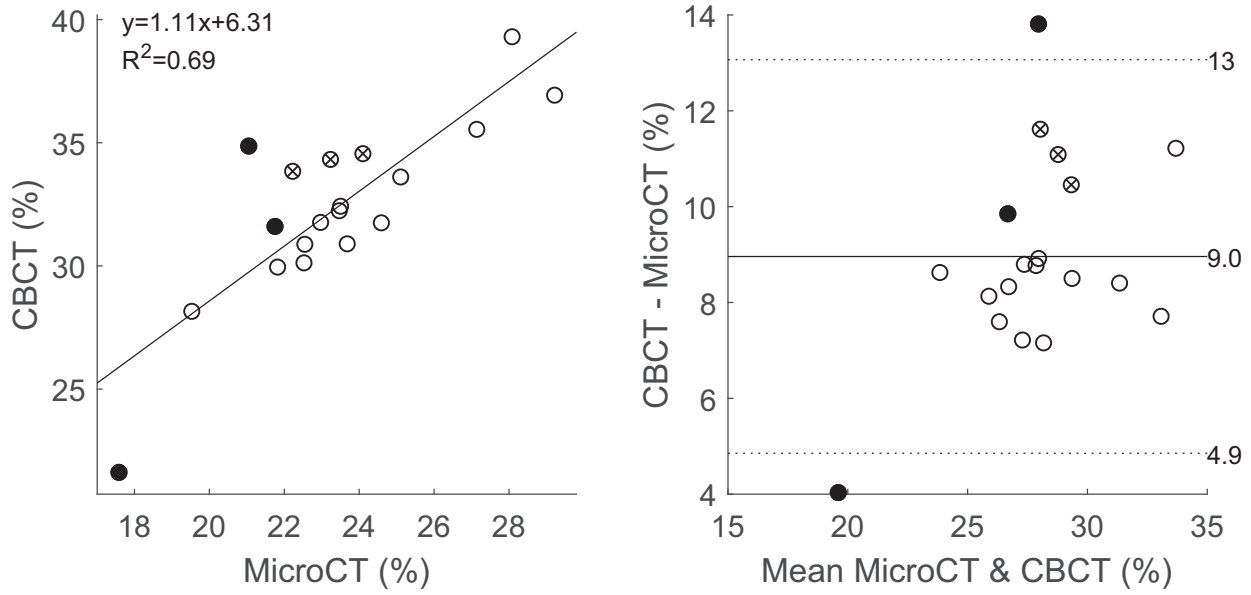

(a) *Percent bone volume (BV/TV)*

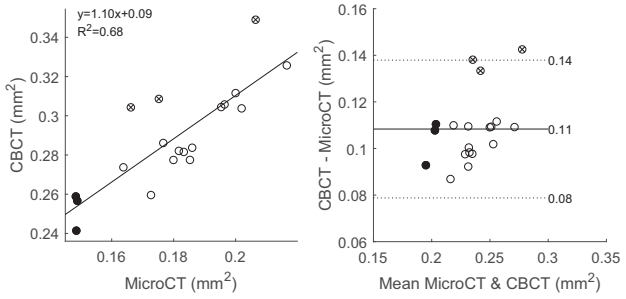

(b) *Trabecular thickness (Tb.Th)*

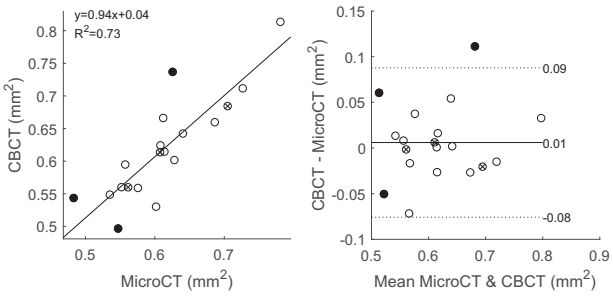

(c) *Trabecular separation (Tb.Sp)*

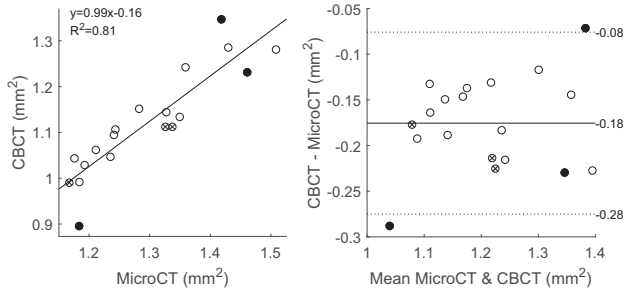

(d) *Trabecular number (Tb.N)*

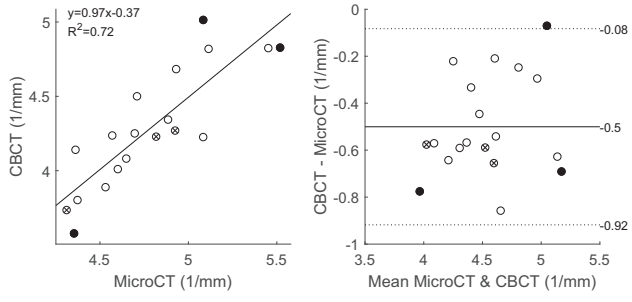

(e) *Bone surface density (BS/TV)*

Fig. 2. Regression plots and Bland Altman plots between MicroCT and RInHouseBeam for bone volume fraction (BV/TV), trabecular thickness (Tb.Th), trabecular separation (Tb.Sp), trabecular number (Tb.N), and bone surface density (BS/TV). Three samples with low trabecular thickness (> 40%of the trabeculae in the VOI thinner than 120 μm) are indicated with filled dots. Three samples that contained a lot of detailed architectural features (almost parallel trabeculae close to each other, small holes and thin, irregular trabeculae) are indicated with a cross.

of determination. Relevant for clinical application is that these trapezia can be detected automatically using the in-house reconstructed CBCT-images; specifically, in RInHouseBeam, these samples have > 19% of trabeculae with a thickness below 180 μm. Hence, for carpal bones with a high ratio of thin trabeculae, the direct method for calculating the parameters should be avoided in clinical practice. We hypothesize that the limit of 120 μm will be lower when scanning radii because these contain more regular trabeculae. Further studies will be performed to test this.

Because of the use of severe osteoarthritic bones, some samples contained trabeculae with small holes inside, nearly parallel trabeculae and very irregular bone structures (Fig. 3) which were undetectable by CBCT. Quantitative analyses showed that the spacings and cavities were often smaller than 60 μm; hence, whereas those trabeculae were treated

Table 3
Relative error (δe) with standard deviation and coefficients of determination between microCT and RManufacturer (standard scanner's reconstruction), RInHouse (in house reconstruction) and RInHouseBeam (in house reconstruction with beam hardening correction). Three bone samples with very low trabecular thickness were excluded ($N = 16$).

	CBCT (N = 16)						
	MicroCT	RManufacturer		RInHouse		RInHouseBeam	
	Mean(SD)	$\delta\epsilon$(SD)	R^2	$\delta\epsilon$(SD)	R^2	$\delta\epsilon$(SD)	R^2
BV/TV [%]	23.98(2.45)	53.11(10.4)%	0.54	46.29(8.6)%	0.68	37.14(6.9)%	0.75
Tb.Th [mm]	0.19(0.01)	109.36(12.0)%	0.53	64.06(9.5)%	0.54	58.50(10.0)%	0.50
Tb.Sp [mm]	0.62(0.07)	8.63(4.7)%	0.85	−5.24(4.3)%	0.86	−0.07(4.9)%	0.83
Tb.N [1/mm]	1.29(0.10)	−26.89(2.5)%	0.80	−10.67(2.8)%	0.83	−13.34(2.6)%	0.86
BS/TV [1/mm]	4.75(0.31)	−28.23(2.8)%	0.62	−10.24(4.0)%	0.66	−10.49(3.8)%	0.69

as two small trabeculae in the microCT-analyses, whereas they were treated as one thick trabecula in CBCT analyses. Especially, three bones (indicated with a cross in Fig. 2) contained a lot of those features and influenced the correlations of Tb.Th and BV/TV significantly. When those bones would not be present in this study, the correlation for Tb.Th would increase from $R^2 = 0.50$ to $R^2 = 0.84$ and for BV/TV from $R^2 = 0.75$ to $R^2 = 0.92$.

It is often claimed that scattering limits the quality of high-resolution CBCT-images [11]. We hypothesize that for small bones such as the trapezium, the partial volume effect and beam hardening effect present the biggest artefacts on the CBCT-images. Indeed, in this study we showed that beam hardening correction enhanced the images tremendously. The partial volume effect was not corrected for.

A potential limitation towards clinical application is that in the present study the bones were scanned in isolation and not in their anatomical configuration. Hence, external artefacts that occur during in vivo scanning were not present. Artefacts due to motion and artefacts due to beam hardening by surrounding bones could potentially deteriorate image quality; in addition, scattering, which is known to increase with increasing object volume, could cause artefacts. These effects will be addressed in subsequent studies.

5. Conclusion

We conclude that bone microarchitecture of fresh-frozen arthritic trapezia of severely osteoarthritic patients can be measured with good accuracy from CBCT-images. We also showed that image quality can be significantly enhanced in comparison with state-of-the-art software,

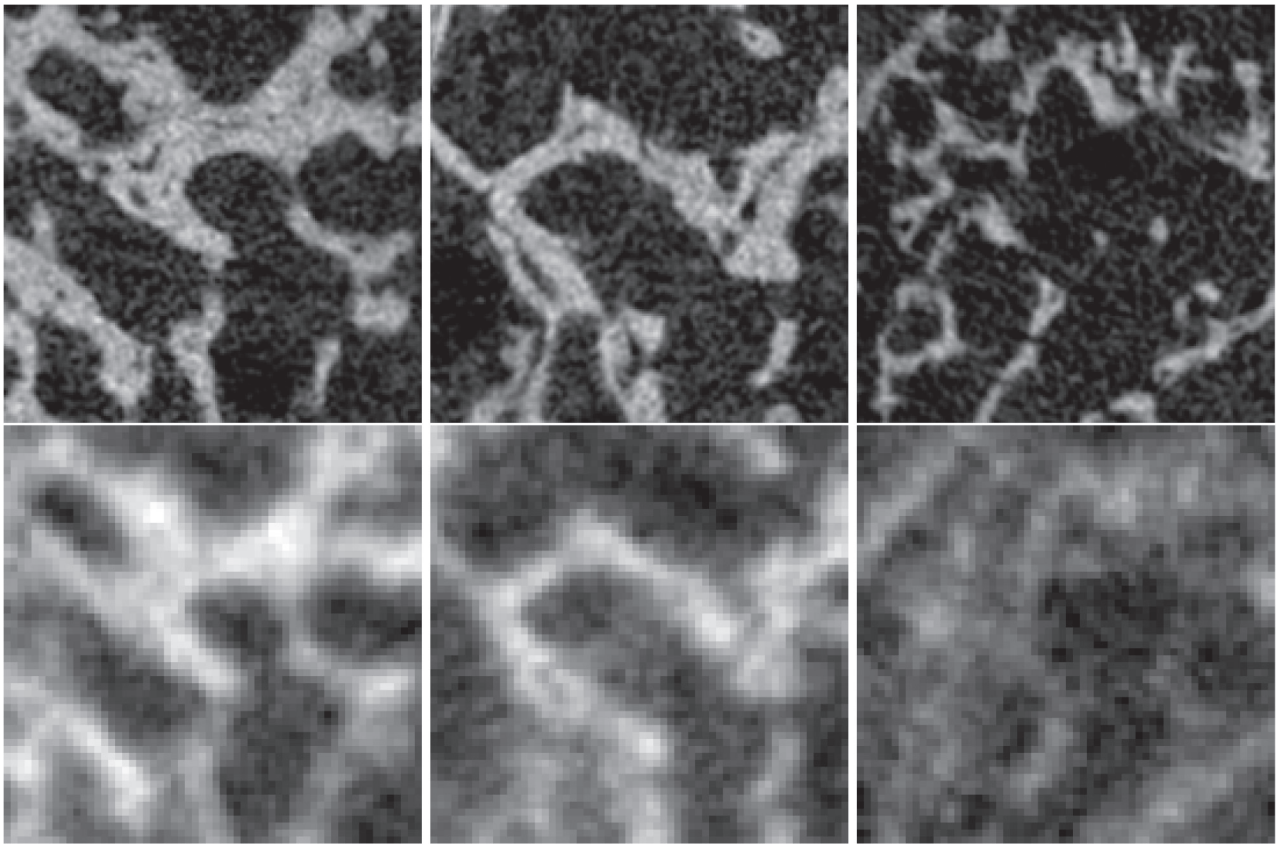

Fig. 3. Small bone features such as small holes in the trabeculae (a), nearly parallel trabeculae close to each other (b) and thin, irregular trabecular structures (c) were observed in the microCT-images (top). The resolution of the CBCT-images (bottom) is too low to depict these features, thus causing morphometric differences between CBCT and microCT.

without a substantial increase in compute time. Further artefact identification and corrections seems useful as well as comparison with HR-pQCT.

We hypothesize that CBCT imaging and analyses could find application in patients with bone diseases such as osteoporosis and osteoarthritis, in the detection of occult fractures which are invisible or doubtful on conventional X-rays, for the visualization of severe fractures to aid surgical intervention and for the follow up of those interventions/fracture repair.

Disclosures

All authors state that they have no conflicts of interest.

Acknowledgments

The project was funded in part by the KU Leuven Internal Funds (C24/16/027). The authors would like to thank Dr. Olivier Vanovermeire for assistance with the CBCT-scans and Haniyeh Hemmatian, PhD, for assistance with the microCT-scans. The authors would like to thank Dr. Walter Coudyzer for providing access to the European Spine Phantom (ESP) and the European Forearm Phantom (EFP) that were used in the initial stage of the study.

Appendix A. Segmentation of CBCT-images

The segmentation of the CBCT-images was performed automatically (Fig. A1). First, a global pre-threshold was performed to delineate a volume of interest (VOI) in which adaptive thresholding was applied. The global pre-threshold was chosen in such a way that all the trabeculae were included. For every voxel in the VOI an adaptive threshold was calculated as the mean of the minimal and maximal values in a sphere with a radius of 6 pixels around the voxel. In parallel, a high global threshold was applied as to include the bone with relatively low grey values that would go unselected by the adaptive segmentation process. Finally, both segmentations were added together and a despeckle of 5 pixels was used to remove the noise.

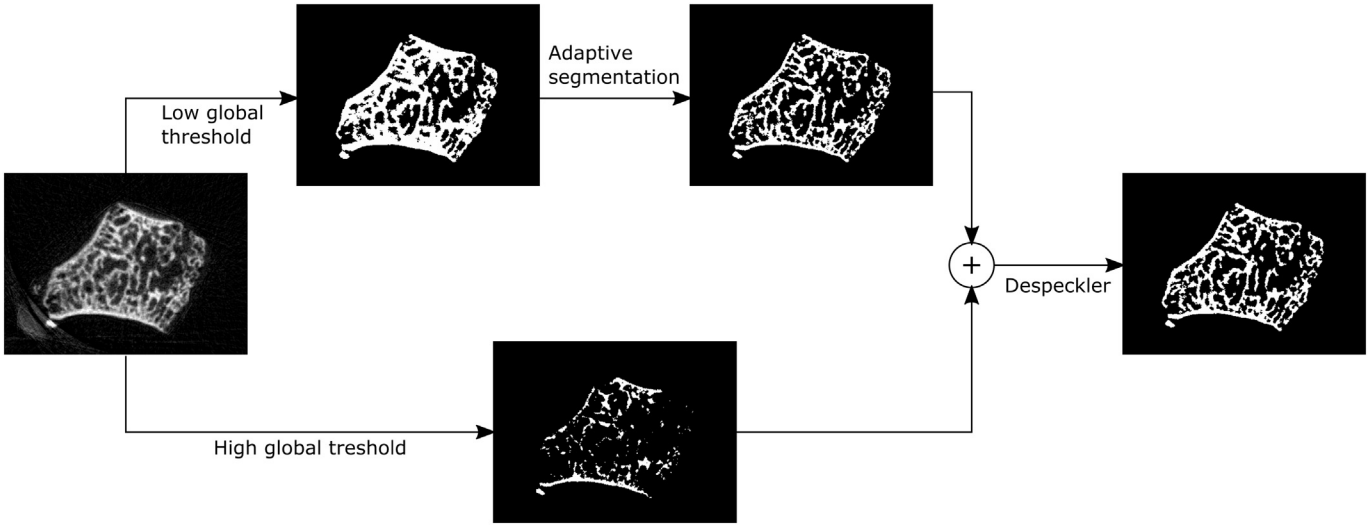

Fig. A1. Automatic segmentation technique for the CBCT-images. The main part consists of a low global threshold, followed by an adaptive segmentation in a sphere with a radius of 6 pixels. In parallel, a high global threshold was applied as to include the bone with relatively low grey values that would go unselected by the adaptive segmentation process. Finally, the noise is reduced with a despeckler.

Appendix B. Automatic calculation of volume of interest based on the microCT-images and registration of the mask on the other images

A trabecular volume of interest (VOI) was selected automatically (Fig. A2) based on the microCT-images, following the method described by Buie et al. [15]. The methodology was adapted (indicated in red in Fig. A3) such that the technique could also be used for bones without a well-defined cortex. In the work of Buie et al. the trabecular mask was determined in a two-step procedure by subtracting the segmented image from the total mask of the bone, followed by a closing operation. We have replaced the first step with two different operations. First, the segmented image was dilated with 3 pixels in order to create a more continuous cortical shell. Afterwards, the dilated segmented image was subtracted from the total mask of the bone. Second, we assumed the thickness of the cortical shell to be at least 6 pixels. These assumptions assured that the trabecular mask would not penetrate into the pores of the cortex. It was implemented by making use of a 6 pixel erosion of the whole mask followed by extraction of this mask.

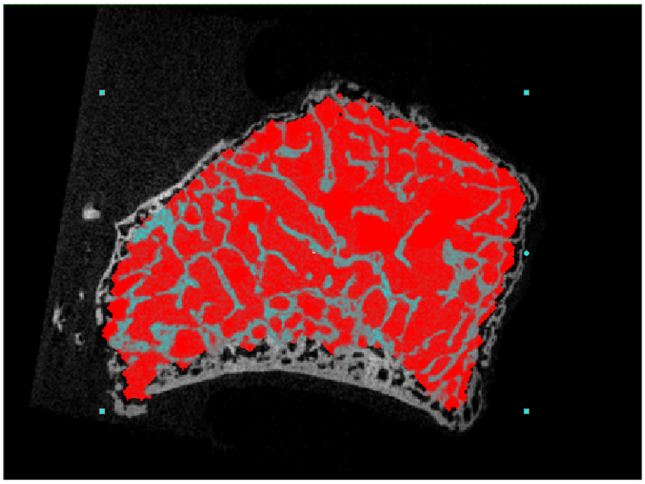

Fig. A2. Depicted in red is one section through the volume of interest (VOI) which was used for the microstructural analyses. This VOI is determined automatically from the microCT-images.

3D intensity-based image registration of the grey value-images was used to select identical trabecular volumes in the CBCT-images. The registration consisted out of four automatic steps and was performed after the correction for beam hardening (RInHouseBeam). First, masks of the whole bones were automatically determined (mask all bone in Fig. A3). Those masks were used to get a rough, but fast, registration of the images. Specifically, the translation between the two masks was calculated based on the center of gravity and the rotation was based on the axes of inertia. Second, the masks were registered using the open-source software Elastix [23, 24]. Third, Elastix was used to perform a precise registration between the grey-level images RInHouseBeam and microCT. Fourth, the inverse transformation was applied to transform the microCT-based trabecular mask onto the CBCT-images.

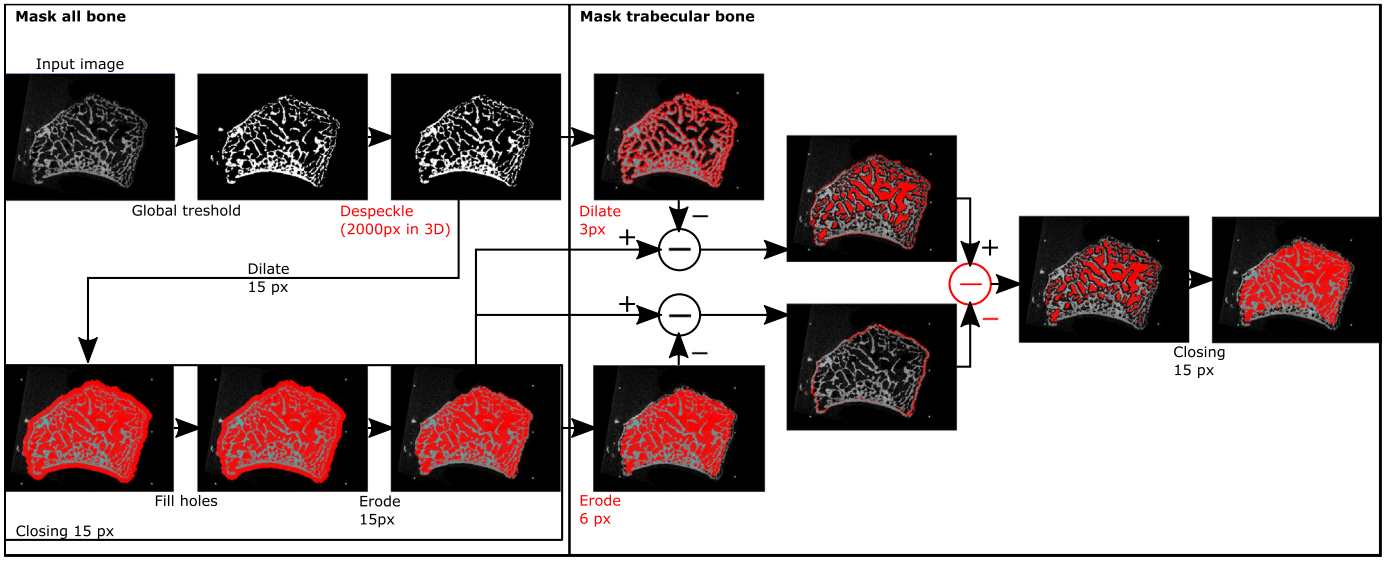

Fig. A3. Automatic determination of the volume of interest (VOI). Based on the method by Buie et al. [14] several steps were added (marked with red labels) to adapt it for the analyses of CBCT-images. (For interpretation of the references to color in this figure legend, the reader is referred to the web version of this article.)

References

[1] E. Hernlund, A. Svedbom, M. Ivergård, J. Compston, C. Cooper, J. Stenmark, E.V. McCloskey, B. Jönsson, J.A. Kanis, Osteoporosis in the European Union: medical management, epidemiology and economic burden: a report prepared in collaboration with the international osteoporosis foundation (IOF) and the European Federation of Pharmaceutical Industry Associations (EFPIA), Arch. Osteoporos. 8 (2013), http://dx.doi.org/10.1007/s11657-013-0136-1.

[2] X.S. Liu, X.H. Zhang, K.K. Sekhon, M.F. Adam, D.J. Mcmahon, J.P. Bilezikian, E. Shane, X.E. Guo, High-resolution peripheral quantitative computed tomography can assess microstructural and mechanical properties of human distal tibial bone, J. Bone Miner. Res. 25 (2009) 746–756, http://dx.doi.org/10.1359/jbmr.090822.

[3] R. Müller, H. Van Campenhout, B. Van Damme, G. Van Der Perre, J. Dequeker, T. Hildebrand, P. Rüegsegger, Morphometric analysis of human bone biopsies: a quantitative structural comparison of histological sections and micro-computed tomography, Bone 23 (1998) 59–66, http://dx.doi.org/10.1016/S8756-3282(98)00068-4.

[4] S. Boutroy, M.L. Bouxsein, F. Munoz, P.D. Delmas, In vivo assessment of trabecular bone microarchitecture by high-resolution peripheral quantitative computed tomography, J. Clin. Endocrinol. Metab. 90 (2005) 6508–6515, http://dx.doi.org/10.1210/jc.2005-1258.

[5] S. Boutroy, B. Van Rietbergen, E. Sornay-Rendu, F. Munoz, M.L. Bouxsein, P.D. Delmas, Finite element analysis based on in vivo HR-pQCT images of the distal radius is associated with wrist fracture in postmenopausal women, J. Bone Miner. Res. 23 (2008) 392–399, http://dx.doi.org/10.1359/jbmr.071108.

[6] N. Vilayphiou, S. Boutruy, E. Sornay-Rendu, B. van Rietbergen, F. Munoz, P.D. Delmas, R. Chapurlat, Finite element analysis performed on radius and tibia HR-pQCT images and fragility fractures at all sites in postmenopausal women, Bone 46 (2010) 1030–1037.

[7] K. Engelke, J.E. Adams, G. Armbrecht, P. Augat, C.E. Bogado, M.L. Bouxsein, D. Felsenberg, M. Ito, S. Prevrhal, D.B. Hans, E.M. Lewiecki, Clinical use of quantitative computed tomography and peripheral quantitative computed tomography in the management of osteoporosis in adults: the 2007 ISCD official positions, J. Clin. Densitom. Assess. Skelet. Heal. 11 (2008) 123–162, http://dx.doi.org/10.

1016/j.jocd.2007.12.010.
[8] W.C. Scarfe, A.G. Farman, P. Sukovic, Clinical applications of cone-beam computed tomography in dental practice, J. Can. Dent. Assoc. 72 (2006) 75–80, http://dx.doi.org/10.1016/j.tripleo.2005.07.027.
[9] J. Koivisto, T. Kiljunen, N. Kadesjö, X.Q. Shi, J. Wolff, Effective radiation dose of a MSCT, two CBCT and one conventional radiography device in the ankle region, J. Foot Ankle Res. 8 (2015), http://dx.doi.org/10.1186/s13047-015-0067-8.
[10] J. De Cock, K. Mermuys, J. Goubau, S. Van Petegem, B. Houthoofd, J.W. Casselman, Cone-beam computed tomography: a new low dose, high resolution imaging technique of the wrist, presentation of three cases with technique, Skelet. Radiol. 41 (2012) 93–96, http://dx.doi.org/10.1007/s00256-011-1198-z.
[11] Y. Huang, J. Van Dessel, M. Depypere, M. Ezeldeen, A.A. Iliescu, E. Dos, Validating cone-beam computed tomography for peri-implant bone morphometric analysis, Bone Res. 2 (2014), http://dx.doi.org/10.1038/boneres.2014.10.
[12] N. Ibrahim, A. Parsa, B. Hassan, P. van der Stelt, I.H.A. Aartman, D. Wismeijer, Accuracy of trabecular bone microstructural measurement at planned dental implant sites using cone-beam CT datasets, Clin. Oral Implants Res. 25 (2014) 941–945, http://dx.doi.org/10.1111/clr.12163.
[13] W. Zbijewski, P. De Jean, P. Prakash, Y. Ding, J.W. Stayman, N. Packard, R. Senn, D. Yang, J. Yorkston, A. Machado, J.A. Carrino, J.H. Siewerdsen, A dedicated cone-beam CT system for musculoskeletal extremities imaging: design, optimization, and initial performance characterization, Med. Phys. 38 (2011) 4700–4713, http://dx.doi.org/10.1118/1.3611039.
[14] S. Lee, C. Lee, H. Cho, H. Park, D. Kim, Y. Choi, H. Kim, L. Seung-Wan, L. Chang-Lae, C. Hyo-Min, P. Hye-Suk, K. Dae-Hong, C. Yu-Na, K. Hee-Joung, Effects of reconstruction parameters on image noise and spatial resolution in cone-beam computed tomography, J. Korean Phys. Soc. 59 (2011) 2825–2832, http://dx.doi.org/10.3938/jkps.59.2825.
[15] H.R. Buie, G.M. Campbell, R.J. Klinck, J.A. MacNeil, S.K. Boyd, Automatic segmentation of cortical and trabecular compartments based on a dual threshold technique for in vivo micro-CT bone analysis, Bone 41 (2007) 505–515, http://dx.doi.org/10.1016/j.bone.2007.07.007.
[17] J.M. Bland, D.G. Altman, Measuring agreement in method comparison studies, Stat. Methods Med. Res. 8 (1999) 135–160, http://dx.doi.org/10.1191/096228099673819272.
[18] J.M. Bland, D.G. Altman, Statistical methods for assessing agreement between two methods of clinical measurement, Lancet 327 (1986) 307–310, http://dx.doi.org/10.1016/S0140-6736(86)90837-8.
[19] E. Klintström, O. Smedby, B. Klintstrom, T.B. Brismar, R. Moreno, Trabecular bone histomorphometric measurements and contrast-to-noise ratio in CBCT, Dentomaxillofac. Radiol. 43 (2014), http://dx.doi.org/10.1259/dmfr.20140196.
[20] J. Van Dessel, L.F. Nicolielo, Y. Huang, W. Coudyzer, B. Salmon, I. Lambrichts, R. Jacobs, Accuracy and reliability of different cone beam computed tomography (CBCT) devices for structural analysis of alveolar bone in comparison with multislice CT and micro-CT, Eur. J. Oral Implantol. 10 (2017) 95–105.
[21] J.A. MacNeil, S.K. Boyd, Accuracy of high-resolution peripheral quantitative computed tomography for measurement of bone quality, Med. Eng. Phys. 29 (2007) 1096–1105, http://dx.doi.org/10.1016/j.medengphy.2006.11.002.
[22] S.L. Manske, Y. Zhu, C. Sandino, S.K. Boyd, Human trabecular bone microarchitecture can be assessed independently of density with second generation HR-pQCT, Bone 79 (2015) 213–221, http://dx.doi.org/10.1016/j.bone.2015.06.006.
[23] D.P. Shamonin, E.E. Bron, B.P.F. Lelieveldt, M. Smits, S. Klein, M. Staring, Fast parallel image registration on CPU and GPU for diagnostic classification of Alzheimer's disease, Front. Neuroinform. 7 (2014), http://dx.doi.org/10.3389/fninf.2013.00050.
[24] S. Klein, M. Staring, K. Murphy, M.A. Viergever, J.P.W. Pluim, Elastix: a toolbox for intensity-based medical image registration, IEEE Trans. Med. Imaging 29 (2010) 196–205, http://dx.doi.org/10.1109/TMI.2009.2035616.